Photocatalysis

International Edition: DOI: 10.1002/anie.201601740
German Edition: DOI: 10.1002/ange.201601740

Plasmonic Nanorattles as Next-Generation Catalysts for Surface Plasmon Resonance-Mediated Oxidations Promoted by Activated Oxygen

*Anderson G. M. da Silva, Thenner S. Rodrigues, Valquírio G. Correia, Tiago V. Alves, Rafael S. Alves, Rômulo A. Ando, Fernando R. Ornellas, Jiale Wang, Leandro H. Andrade, and Pedro H. C. Camargo**

Abstract: *Nanorattles, comprised of a nanosphere inside a nanoshell, were employed as the next generation of plasmonic catalysts for oxidations promoted by activated O_2. After investigating how the presence of a nanosphere inside a nanoshell affected the electric-field enhancements in the nanorattle relative to a nanoshell and a nanosphere, the SPR-mediated oxidation of p-aminothiophenol (PATP) functionalized at their surface was investigated to benchmark how these different electric-field intensities affected the performances of Au@AgAu nanorattles, AgAu nanoshells and Au nanoparticles having similar sizes. The high performance of the nanorattles enabled the visible-light driven synthesis of azobenzene from aniline under ambient conditions. As the nanorattles allow the formation of electromagnetic hot spots without relying on the uncontrolled aggregation of nanostructures, it enables their application as catalysts in liquid phase under mild conditions using visible light as the main energy input.*

Oxidation reactions play a pivotal role in industrial processes and academic research,[1–3] in which the activation of molecular oxygen (O_2) at the catalyst surface represents a promising alternative to achieve high activities.[4–6] Interestingly, it has been demonstrated that the surface plasmon resonance (SPR) excitation in silver (Ag) and gold (Au) nanostructures can generate activated O_2 at the metal surface.[7–12] This process occurs through the charge transfer of SPR-excited hot electrons to adsorbed O_2 molecules, allowing the use of visible-light to drive oxidation reactions.[7–12]

Most studies on SPR-mediated transformations have focused on first-generation plasmonic catalysts, that is, conventional Ag and Au nanoparticles such as quasi-spheres, cubes, wires, plates, among others.[7–12] Herein, we propose the utilization of metallic nanorattles, comprised of a nanosphere inside of a nanoshell, as the next generation of plasmonic catalysts towards SPR-mediated oxidations by taking advantage of the plasmon hybridization concept.[13,14] In nanorattles, plasmon hybridization between the nanoshell and nanosphere components can lead to much higher electric field (E-field) enhancements relative to its individual counterparts.[15–17] Nanorattles also enable the generation of electromagnetic hot spots in a controllable manner without relying on the uncontrolled aggregation among individual nanostructures.[18,19] This is not possible in first-generation plasmonic catalysts, and aggregation leads to a decrease in surface area and thus catalytic performance. Previously, high efficiencies towards SPR-mediated transformations were described at junctions between Ag nanocubes supported over Al_2O_3.[20] Although these junctions could present higher E-field enhancements relative to the nanorattles, their formation still relies on the uncontrolled aggregation and the synthesis of nanocubes is more complex relative to spherical nanoparticles. Finally, procedures for the synthesis of nanorattles have been reported, and their optical properties can be easily tuned as a function of size and wall-thickness.[14,21,22]

Theoretical simulations indicate that the $|E_{max}|^2/|E_0|^2$ values were significantly higher for a nanorattle as compared to a nanoshell and a nanosphere having similar sizes (see Figures S1 and S2 in the Supporting Information). In our calculations, the nanorattle dimensions corresponded to 40 nm in outer diameter, 5 nm in shell thickness, and contained a nanosphere 20 nm within its void. The $|E_{max}|^2/|E_0|^2$ values at 633 nm excitation corresponded to 570.30 and 867.10 (polarization along the *y*- and *z*-axis, respectively) for the nanorattle, 49.87 for the nanoshell, and 11.26 for the nanosphere, indicating that $|E_{max}|^2/|E_0|^2$ for the nanorattle was up to 14-fold higher relative to the nanoshell and nanosphere. This observation is in agreement with previous reports,[13,14] and originates from the plasmon hybridization between the nanoshell and nanosphere,[13,23] in which the plasmon modes of the elementary nanoparticles combine leading to increased electric field intensities at the junction of neighboring nanoparticles, that is, the so-called electromagnetic hot spots.[14] The calculated UV/Vis extinction spectra for the nanorattle, nanoshell and nanosphere are shown in Figure S3A–C, respectively, and agree with the plasmon hybridization phenomenon. While the spectra for the nanoshell and nanosphere displayed single bands centered at 508 and 576 nm, respectively, the spectra for the nanorattle was comprised of a shoulder around 500–600 nm

[*] A. G. M. da Silva, T. S. Rodrigues, V. G. Correia, T. V. Alves, R. S. Alves, R. A. Ando, F. R. Ornellas, J. Wang, L. H. Andrade, P. H. C. Camargo
Instituto de Química, Universidade de São Paulo
Av. Prof. Lineu Prestes, 748, 05508-000, São Paulo-SP (Brazil)
E-mail: camargo@iq.usp.br
J. Wang
College of Science, Donghua University
Shanghai 201620 (P.R. China)

Supporting information for this article, including experimental methods, theoretical simulations, calculated UV/Vis spectra, additional SERS, NMR, mass, and UV/Vis spectra, can be found under: http://dx.doi.org/10.1002/anie.201601740.

and a band at 630 nm.[14,22] It is important to note that $|E_{max}|^2/|E_0|^2$ values for the nanoshell and nanospheres employing 576 and 508 nm as the excitation wavelength, respectively, corresponded to 15.01 and 53.73, being still inferior to that observed for the nanorattles under 633 nm excitation.

In order to experimentally investigate how the increased E-field enhancements observed for the nanorattle can be employed to achieve higher SPR-mediated performances relative to a nanoshell and a nanosphere, we synthesized Au@AgAu nanorattles as well as their AgAu nanoshells and Au nanoparticles counterparts having similar sizes (Scheme S1).[24] The Au@AgAu nanorattles were 39 ± 5 nm in outer diameter and about 5 nm in shell thickness, while the size of the Au nanoparticles located inside the voids corresponded to 19 ± 3 nm (Figure 1 A and D). Likewise,

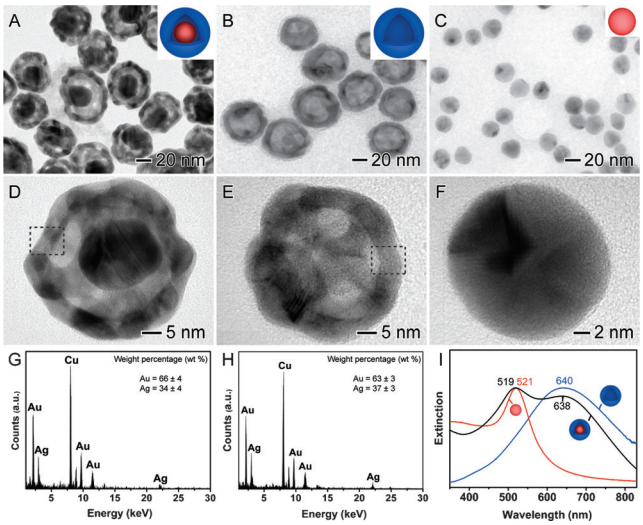

Figure 1. A–C) TEM and D–F) HRTEM images for Au@AgAu nanorattles (A and D), AgAu nanoshells (B and E), and Au nanoparticles (C and F). The EDX spectra from the regions indicated by black dashed squares in (D) and (E) are shown in (G) and (H), respectively. I) Normalized UV/Vis extinction spectra recorded from aqueous suspensions containing Au@AgAu nanorattles, AgAu nanoshells and Au nanoparticles (black, blue, and red traces, respectively).

the AgAu nanoshells were 38 ± 4 nm in outer diameter and 5 nm in shell thickness (Figure 1 B and E). Figure 1 C and F show TEM and HRTEM images of Au nanoparticles employed as seeds for the synthesis of the nanorattles. They were 19 ± 3 nm in diameter.

The EDX spectra registered from the regions indicated by black dashed rectangles (Figure 1 G and H, respectively) confirmed that the nanorattles and nanoshells display similar wall compositions (66 ± 4 and 63 ± 3 Au wt. %, respectively). Figure 1 I depicts the UV/Vis extinction spectra recorded from aqueous suspensions containing the Au@AgAu nanorattles, AgAu nanoshells, and Au nanoparticles (black, blue, and red traces, respectively). The spectra for AgAu nanoshells and Au nanoparticles displayed one dipole mode LSPR extinction band centered at 640 and 521 nm,[25,26] respectively. Conversely, the presence of two extinction bands at 519 and 638 nm was observed for the nanorattles. This is in agreement with the calculated spectra shown in Figure S3.

In the next step, we were interested in the following question: would the higher E-field enhancements enabled by the nanorattle morphology relative to nanoshells and nanospheres translate into improved properties in SPR-mediated transformations? In order to address this challenge, we employed SPR-mediated oxidation of PATP functionalized at the surface of the nanomaterials as a proof-of-concept transformation to benchmark the performance of the nanorattles relative to nanoshells and nanospheres according to the following Equation (1).[10,27]

$$2\,\text{AuS-Ph-NH}_2 + \text{O}_2 + h\nu \rightarrow \text{AuS-Ph-N=N-Ph-SAu} + 2\,\text{H}_2\text{O} \qquad (1)$$

It has been proposed that this reaction takes place as SPR-excited hot electrons are transferred to adsorbed O_2 molecules (from air). This leads to the generation of $^{-}O_2$ species which participate in the PATP oxidation.[10] This model reaction can be monitored in a Raman spectrometer, in which the incoming laser is employed as both the excitation source and to monitor the DMAB formation by SERS.[8,10] Interestingly, both PATP and DMAB adsorb strongly on Ag and Au surfaces via M-S covalent bonds, leading to the formation of a monolayer which enable PATP molecules to be in close proximity at the surface in all nanostructures.[8,10] Therefore, due to the formation of a monolayer at the surface, it is plausible that in all nanoparticles the probability for two neighboring PATP molecules to interact should be similar.

Figure 2 A and B show the SERS spectra registered from Au@AgAu nanorattles that had been functionalized with PATP as a function of the laser power (Figure 2 A) and exposure time (Figure 2 B). The bands assigned to PATP and DMAB could be clearly detected in all spectra: the bands at 1081, 1188, 1489, and 1593 cm^{-1} corresponded to A_1 modes of

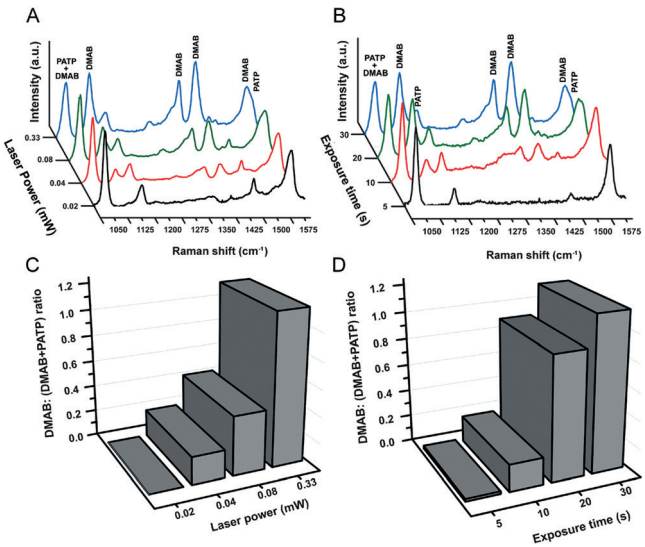

Figure 2. Laser-power (A) and irradiation-time (B) dependent SERS spectra for Au@AgAu nanorattles that had been functionalized with PATP employing 30 s as the exposure time (A) and 0.33 mW as the laser power (B). C,D) show the DMAB:(DMAB + PATP) 1433:1081 intensity ratios obtained from (A) and (B), respectively.

PATP while the bands at 1081, 1142, 1390, 1433, and 1575 cm^{-1} were assigned to the A_g modes of DMAB.[28] The intensities of the DMAB bands as well as DMAB:(DMAB + PATP) 1433:1081 intensity ratios (plotted in Figure 2C and D) increased with the laser power and exposure time in agreement with a SPR-mediated reaction mechanism.[29] The same laser-power dependency behavior was observed for the Au nanoparticles and AgAu nanoshells (Figure S4A and S4B, respectively). Although localized heating due to SPR excitation can contribute to the oxidation reaction, the absence of an exponential dependence between laser power (illumination intensity) and photocatalytic rate suggests that the reaction was not driven by a thermal process, in agreement with an electron driven pathway in which hot electrons are transferred to adsorbed O_2 species.[30] In this context, it has been demonstrated that macroscopically observable photocatalytic rate dependence on illumination intensity can provide important mechanistic insights over the transformations mediated by the SPR excitation.[30] Specifically, while exponential relationships between photon-induced rates and illumination intensities can be associated with mechanisms that are driven by a thermal process, a linear rate dependence on intensity is associated with an electron driven process.[30]

Figure 3A displays the SERS spectra acquired from nanorattles, nanoshells, and nanoparticles that had been

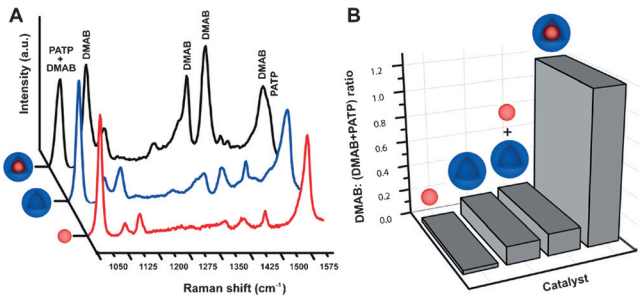

Figure 3. SERS spectra (A) and DMAB:(DMAB + PATP) 1433:1081 intensity ratios (B) for Au@AgAu nanorattles (black trace), AgAu nanoshells (blue trace), and Au nanoparticles (red trace) that had been functionalized with PATP employing 30 s as the exposure time and 0.33 mW as the laser power.

functionalized with PATP employing 0.33 mW as the laser power and 30 s as the acquisition time (these conditions correspond to the point at which the PATP to DMAB conversion was maximized in all cases). The intensity of the DMAB signals as well as the relative DMAB:(DMAB + PATP) 1433:1081 intensity ratios (Figure 3B) were significantly higher for the nanorattles as compared to the nanoshells and nanoparticles. Specifically, the DMAB:(PATP + DMAB) 1433:1081 intensity ratios turned out to be 1.19, 0.13, and 0.03 for the nanorattles, nanoshells, and nanoparticles, respectively. This represents an increase of 9.2- and 40-fold in the PATP conversion for the nanorattles compared to the nanoshells and nanoparticles, respectively, and an enhancement of 7.4-fold relative to the sum of nanoshell and nanosphere performances.

After demonstrating that the higher E-field enhancements as enabled by plasmon hybridization in the nanorattle structure led to remarkably higher SPR-mediated oxidation of PATP functionalized at the surface, we turned our attention to the utilization of the nanorattles as plasmonic catalysts for the oxidation of aniline driven by visible-light under ambient conditions as shown in Figure 4A (room temperature, 1 atm

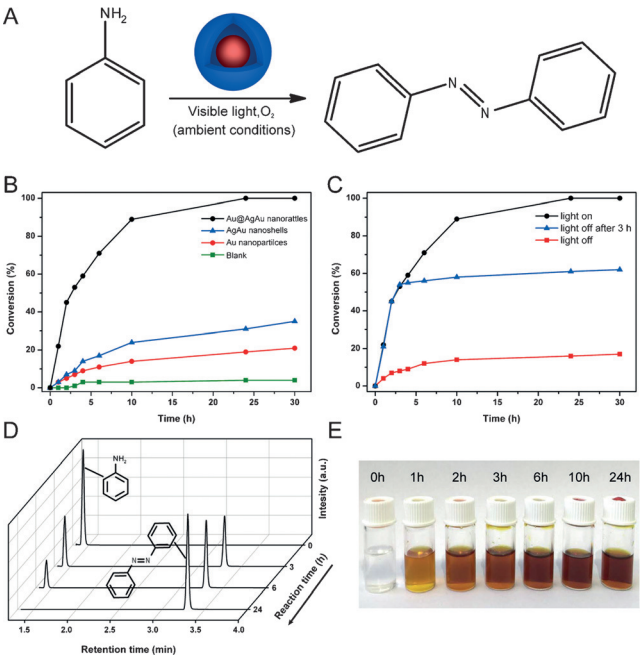

Figure 4. A) SPR-mediated oxidation of aniline catalyzed by the nanorattles. B) Conversion (%) of aniline as a function of time catalyzed by Au@AgAu nanorattles, AgAu nanoshells, and Au nanoparticles (black, blue, and red traces, respectively) C) Conversion (%) of aniline employing nanorattles as catalysts in the absence of visible light or by turning the light off after 3 h. Chromatograms (D) and digital photographs (E) obtained from the reaction mixture solutions catalyzed by the nanorattles as a function of time.

of O_2, and employing a 300 W tungsten lamp as the excitation source). As the visible-light excitation comprises the entire visible region, it can excite the SPR of nanorattles, nanoshells, and nanoparticles (whose SPR maxima are centered at different laser wavelengths). This, in turn, allowed us to systematically investigate the concept of plasmon hybridization in Au@AgAu nanorattles towards SPR-mediated oxidation reactions promoted by activated O_2. It is noteworthy that the conventional synthesis of aromatic azocompounds from amines requires several reaction steps and stoichiometric amounts of nitrite salts ($NaNO_2$) as well as toxic oxidants.[31] Although the use of inorganic oxides and metal nanoparticles as catalysts to produce azobenzene in good yields has been reported, the utilization of harsh conditions (strong oxidizing agents, high pressures of O_2 and/or temperatures up to 150 °C) are still required.[31–34]

Figure 4B shows the conversion (%) for the oxidation of aniline as a function of time by employing the Au@AgAu nanorattles (black trace), AgAu nanoshells (blue trace), and Au nanoparticles (red trace) as catalyst. The utilization of the

Au@AgAu nanorattles led to > 90 % of conversion after 10 h. This conversion (%) was significantly higher relative to nanoshells and nanoparticles (23 and 14 %, respectively). The temperature of the reaction mixture at the end of the reaction corresponded to 34° C and no significant conversion was obtained in the absence of any catalyst (blank reaction, green trace). The orange trace depicts the conversion (%) considering the sum of AgAu nanoshells and Au NPs. Here, as all the catalytic experiments were carried out under the same loading of nanoparticles, their dimensions are comparable, and the shells have similar compositions, the variations in the catalytic performances of the nanorattles relative to the sum of nanoshells and nanoparticles enables us to isolate the contribution of the SPR excitation over the catalytic performance, as the same amount of surface area is available in this case. It can be observed that, after 10 h, the conversion (%) for the nanorattles was 3-fold higher relative to the sum of nanoshells and nanoparticles (same available surface areas), confirming the role of the SPR excitation over the enhancement of catalytic activities in the nanorattles.

In order to demonstrate that this transformation was mediated by the SPR excitation in the Au@AgAu nanorattles and estimate the contribution from external heating, we compared the conversion (%) with and without the visible-light excitation as shown in Figure 4 C. Low conversion (%) were obtained without visible-light excitation (red trace, employing 34 °C as the reaction temperature). Specifically, only 15 % of conversion was observed after 10 h as compared to > 90 % under visible-light excitation (black trace). The role of visible-light excitation was further confirmed by monitoring the catalytic conversion under visible-light excitation for 3 h and then turning off the light source as depicted in Figure 4 D, blue trace. In this case, no significant conversion took place after the light source was turned off. In order to gain further insights over the contribution of external heating, we also performed control experiments at 60 and 80 °C (without light excitation) and no improvement in the conversion (%) were observed as compared to the reaction performed at 34° C. This is in agreement with previous results and reports demonstrating that the reaction occurs via an electron transfer mechanism.[10,31]

Encouragingly, only azobenzene was detected as reaction product as confirmed by the chromatograms collected from the reaction mixture at different times intervals, which revealed the gradual aniline consumption and concomitant appearance of a single reaction product as depicted in Figure 4 D. Figure 4 E shows the digital photographs from the reaction mixture isolated at different time-intervals, which shows the gradual appearance of an orange-red color in the solution that is characteristic of the azobenzene formation. The chemical structure of azobenzene was confirmed by CG-MS, RMN and UV/Vis analyses from the isolated product (Figures S5–S8). No aniline conversion was detected when the reaction was carried out in the absence of O_2. Moreover, the utilization of air (instead of O_2) led to a decrease in the conversion (%) by 3-fold.

Scheme 1 shows the proposed mechanism for the SPR-mediated oxidation of aniline catalyzed by the plasmonic nanorattles according to what has been established in the literature and our reported results.[10,31,35–37] First, $^{-}O_2$ species are generated from SPR excitation (Scheme 1 A). Then, these species enter the catalytic cycle (Scheme 1 B) and oxidize the nitrogen atom of aniline, leading to an aniline radical cation ($^{-}O_2$ molecules often lead to radical mechanism). In the next step, the coupling between the aniline radical cation and an aniline molecule may lead to the formation of a three-electron σ bond intermediate. This intermediate could lose hydrogen atoms in the presence of OH^{-}(aq) species forming H_2O. This is supported by the fact that the formation of azobenzene could not detected when the reaction was carried out in the absence of OH^{-}(aq).[38] Finally, the produced hydrazine can quickly be converted to azobenzene product by a superoxide species regenerating the catalyst. In order to check the reusability of the nanorattles as catalyst, they were recovered from the reaction mixture by centrifugation at the end of the reaction. The recovered catalyst could be re-used at least three times without a significant loss of performance (96 % of conversion after the 3rd cycle). It is important to note that, although the local electromagnetic field generated due to plasmon hybridization in the nanorattles is within the void region, they can contribute the described oxidation processes

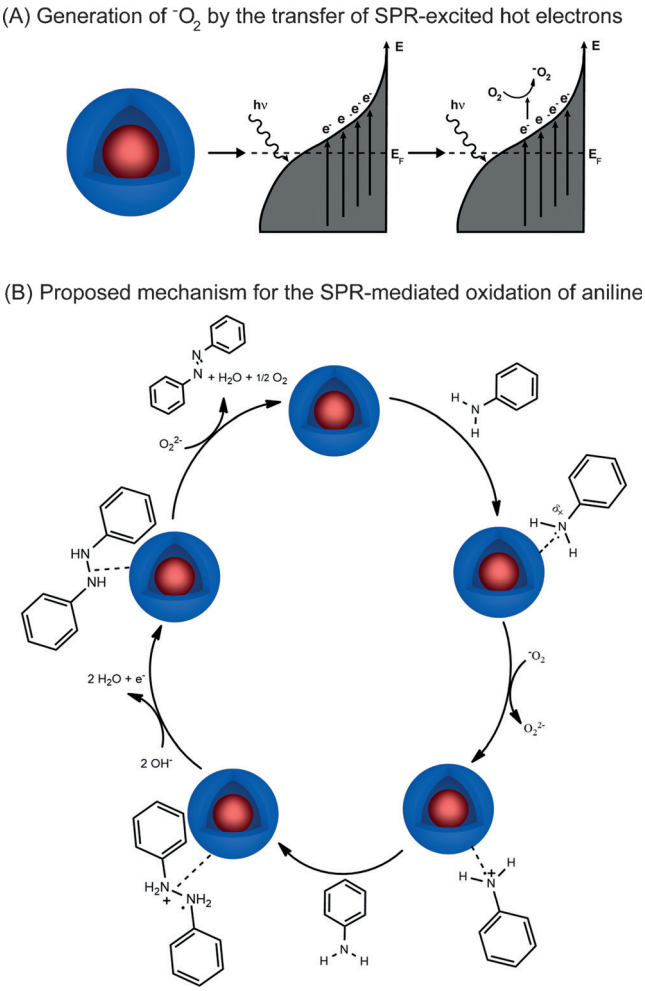

Scheme 1. Proposed mechanism for the SPR-mediated oxidation of aniline. After $^{-}O_2$ species are generated as a result of SPR excitation (A), they participate in the catalytic cycle by a radical mechanism (B).

as the nanorattles outer shell is porous and enable the diffusion of molecules to their interior (Figures S9 and S10).[39] Moreover, as the SPR catalytic properties are strongly dependent on size and optical properties, the control over the nanorattle dimensions (such as shell thickness, void gap, and Au nanoparticles size) may be employed to further optimize the catalytic performances.

In summary, we demonstrated that the concept of plasmon hybridization in Au@AgAu nanorattles led to improved performances towards SPR-mediated oxidation reactions promoted by activated O_2. Firstly, we compared the E-field enhancements for the nanorattles relative to nanoshells and nanospheres and benchmarked their performances using the oxidation of PATP functionalized at the surface as a proof-of-concept transformation. Then, the nanorattles were employed as plasmonic catalysts to the synthesis of azobenzene from aniline under ambient conditions. As the nanorattle morphology enables the formation of electromagnetic hot spots, in a well-defined and controlled manner (as opposed to the uncontrolled aggregation of nanoparticles), they represent the next-generation of plasmonic catalysts for applications in oxidation reactions and potentially other transformations.

Acknowledgements

This work was supported by FAPESP (grant numbers 2013/19861-6 and 2015/21366-9). F.R.O., L.H.A., and R.A.A. thank the CNPq for the research fellowships. A.G.M.S., T.S.R, J.W., V.G.C., T.V.A., and R.S.A. thank CNPq, FAPESP and CAPES for the fellowships.

Keywords: photocatalysis · nanorattles · oxidation · plasmonics · surface plasmon resonances

How to cite: *Angew. Chem. Int. Ed.* **2016**, *55*, 7111 – 7115
Angew. Chem. **2016**, *128*, 7227 – 7231

[1] F. Zaera, *Chem. Soc. Rev.* **2013**, *42*, 2746 – 2762.
[2] M. Stratakis, H. Garcia, *Chem. Rev.* **2012**, *112*, 4469 – 4506.
[3] A. G. M. da Silva, C. M. Kisukuri, T. S. Rodrigues, E. G. Candido, I. C. de Freitas, A. H. M. da Silva, J. M. Assaf, D. C. Oliveira, L. H. Andrade, P. H. C. Camargo, *Appl. Catal. B* **2016**, *184*, 35 – 43.
[4] R. Long, K. Mao, X. Ye, W. Yan, Y. Huang, J. Wang, Y. Fu, X. Wang, X. Wu, Y. Xie, et al., *J. Am. Chem. Soc.* **2013**, *135*, 3200 – 3207.
[5] A. P. Woodham, G. Meijer, A. Fielicke, *Angew. Chem. Int. Ed.* **2012**, *51*, 4444 – 4447; *Angew. Chem.* **2012**, *124*, 4520 – 4523.
[6] C. S. Hinde, D. Ansovini, P. P. Wells, G. Collins, S. Van Aswegen, J. D. Holmes, T. S. A. Hor, R. Raja, *ACS Catal.* **2015**, *5*, 3807 – 3816.
[7] P. Christopher, H. Xin, S. Linic, *Nat. Chem.* **2011**, *3*, 467 – 472.
[8] J. Wang, R. A. Ando, P. H. C. Camargo, *Angew. Chem. Int. Ed.* **2015**, *54*, 6909 – 6912; *Angew. Chem.* **2015**, *127*, 7013 – 7016.
[9] J. L. Wang, R. A. Ando, P. H. C. Camargo, *ACS Catal.* **2014**, *4*, 3815 – 3819.
[10] Y.-F. Huang, M. Zhang, L.-B. Zhao, J.-M. Feng, D.-Y. Wu, B. Ren, Z.-Q. Tian, *Angew. Chem. Int. Ed.* **2014**, *53*, 2353 – 2357; *Angew. Chem.* **2014**, *126*, 2385 – 2389.
[11] A. G. M. da Silva, T. S. Rodrigues, J. Wang, L. K. Yamada, T. V. Alves, F. R. Ornellas, R. A. Ando, P. H. C. Camargo, *Langmuir* **2015**, *31*, 10272 – 10278.
[12] L.-B. Zhao, M. Zhang, Y.-F. Huang, C. T. Williams, D.-Y. Wu, B. Ren, Z.-Q. Tian, *J. Phys. Chem. Lett.* **2014**, *5*, 1259 – 1266.
[13] E. Prodan, C. Radloff, N. J. Halas, P. Nordlander, *Science* **2003**, *302*, 419 – 422.
[14] M. A. Mahmoud, *J. Phys. Chem. Lett.* **2014**, *5*, 2594 – 2600.
[15] K.-K. Liu, S. Tadepalli, L. Tian, S. Singamaneni, *Chem. Mater.* **2015**, *27*, 5261 – 5270.
[16] M. A. Mahmoud, *J. Phys. Chem. C* **2014**, *118*, 10321 – 10328.
[17] Y. Khalavka, J. Becker, C. Sönnichsen, *J. Am. Chem. Soc.* **2009**, *131*, 1871 – 1875.
[18] S. L. Kleinman, R. R. Frontiera, A.-I. Henry, J. A. Dieringer, R. P. Van Duyne, *Phys. Chem. Chem. Phys.* **2013**, *15*, 21 – 36.
[19] M. A. Mahmoud, M. A. El-Sayed, *Nano Lett.* **2009**, *9*, 3025 – 3031.
[20] P. Christopher, H. Xin, A. Marimuthu, S. Linic, *Nat. Mater.* **2012**, *11*, 1044 – 1050.
[21] Y. Sun, B. Wiley, Z.-Y. Li, Y. Xia, *J. Am. Chem. Soc.* **2004**, *126*, 9399 – 9406.
[22] M. Priebe, K. M. Fromm, *Chem. Eur. J.* **2015**, *21*, 3854 – 3874.
[23] P. Nordlander, E. Prodan, *Nano Lett.* **2004**, *4*, 2209 – 2213.
[24] X. Xia, Y. Wang, A. Ruditskiy, Y. Xia, *Adv. Mater.* **2013**, *25*, 6313 – 6333.
[25] S. E. Skrabalak, J. Chen, Y. Sun, X. Lu, L. Au, C. M. Cobley, Y. Xia, *Acc. Chem. Res.* **2008**, *41*, 1587 – 1595.
[26] N. R. Jana, L. Gearheart, C. J. Murphy, *Langmuir* **2001**, *17*, 6782 – 6786.
[27] M. Sun, H. Xu, *Small* **2012**, *8*, 2777 – 2786.
[28] L. Kang, P. Xu, B. Zhang, H. Tsai, X. Han, H.-L. Wang, *Chem. Commun.* **2013**, *49*, 3389 – 3391.
[29] S. Linic, P. Christopher, D. B. Ingram, *Nat. Mater.* **2011**, *10*, 911 – 921.
[30] M. J. Kale, T. Avanesian, P. Christopher, *ACS Catal.* **2014**, *4*, 116 – 128.
[31] B. Dutta, S. Biswas, V. Sharma, N. O. Savage, S. P. Alpay, S. L. Suib, *Angew. Chem. Int Ed.* **2016**, *55*, 2171 – 2175; *Angew. Chem.* **2016**, *128*, 2211 – 2215.
[32] K. Monir, M. Ghosh, S. Mishra, A. Majee, A. Hajra, *Eur. J. Org. Chem.* **2014**, 1096 – 1102.
[33] A. Grirrane, A. Corma, H. García, *Science* **2008**, *322*, 1661 – 1664.
[34] S. Ghosh, S. S. Acharyya, T. Sasaki, R. Bal, *Green Chem.* **2015**, *17*, 1867 – 1876.
[35] S. Cai, H. Rong, X. Yu, X. Liu, D. Wang, W. He, Y. Li, *ACS Catal.* **2013**, *3*, 478 – 486.
[36] P. Xu, L. Kang, N. H. Mack, K. S. Schanze, X. Han, H.-L. Wang, *Sci. Rep.* **2013**, *3*, 2997.
[37] D.-Y. Wu, L.-B. Zhao, X.-M. Liu, R. Huang, Y.-F. Huang, B. Ren, Z.-Q. Tian, *Chem. Commun.* **2011**, *47*, 2520 – 2522.
[38] X. Hong, D. Wang, S. Cai, H. Rong, Y. Li, *J. Am. Chem. Soc.* **2012**, *134*, 18165 – 18168.
[39] T. J. A. Slater, A. Macedo, S. L. M. Schroeder, M. G. Burke, P. O'Brien, P. H. C. Camargo, S. J. Haigh, *Nano Lett.* **2014**, *14*, 1921 – 1926.

Received: February 18, 2016
Published online: May 9, 2016

